RSC Advances

ROYAL SOCIETY OF CHEMISTRY

www.rsc.org/advances

Table of Contents Entry

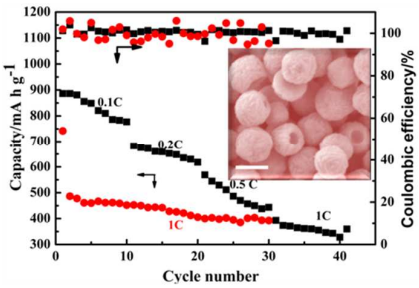

The as-obtained FeS_2 hollow microsphere electrode delivered excellent cycling stability and electrochemical performance after the first cycle at ambient temperature.

Cite this: DOI: 10.1039/c0xx00000x

www.rsc.org/xxxxxx

ARTICLE TYPE

Hierarchical nanostructured FeS_2 hollow microspheres for lithium-ion batteries

Yourong Wang, Xiaofang Qian,Wei Zhou, Hantao Liao and Siqing Cheng*

Received (in XXX, XXX) Xth XXXXXXXXX 20XX, Accepted Xth XXXXXXXXX 20XX

DOI: 10.1039/b000000x

The hierarchical nanostructured FeS_2 hollow microspheres composed of nanoflakes were fabricated based on Ostwald ripening using the sulfur powder as sulfur source and triethanolamine as both solvent and reducing agent, and electrochemically investigated as cathode material for lithium ion battery. The as-obtained FeS_2 electrode delivered an initial capacity of 886.3 mAh g^{-1} at 0.1 C at ambient temperature, which is one of the highest values in the reported results. In the subsequent cycles followed by the first cycle, the electrode exhibited good reversibility at ambient temperature, resulting in good cycling stability and performance, and the discharge capacity of 392.7 mAh g^{-1} at 1C was still retained after 30 cycles. This might be attributed to the unique FeS_2 structure with hierarchical nanostructured hollow microsphere, showing potential to develop the FeS_2 cathode materials with the high energy density for lithium ion battery.

Introduction

Iron pyrite (cubic β-FeS_2, "fool's gold", hereafter termed pyrite for simplicity) is an under-researched semiconductor that is extremely promising for both solar energy conversion [1–4] and electrochemical energy storage[5–7]. Concerning photovoltaics, pyrite's unique properties include an exceptionally large optical absorption coefficient in the visible region ($\alpha > 10^{-5}$ cm^{-1} at $hv >$ 1.3 eV), desirable band gap of 0.95 eV for a solar spectrum and a maximum of 28% theoretical photovoltaic efficiency based on Shockley-Queisser estimate[1], coupled with large elemental abundances, nontoxicity and low material refinement costs, which boosts a great deal of interest in investigating pyrite as a thin light absorber for photovoltaic and photoelectrochemical application, since Tributsch[8] first demonstrated pyrite photoelectrochemical and schottky solar cells in 1984. Specially, pyrite nanocrystals with various morphologies, for example nanotubes[2,9], nanorods[10,11], nanosheets[12,13], nanowires[13–16], nanospheres[13], nanoplates[11,13], have been advanced in order to vary the band gap of pyrite for harvesting broad spectrum of light with wavelengths as long as 750 nm. It is comparatively less well known that pyrite is also one of the best candidate cathode materials for LIBs[5–7], especially for applications in EV (electric vehicles) / HEVs (hybrid electric vehicles) due to its high theoretical capacity of 890 mAh g^{-1} and the high theoretical energy density of 1273 Wh kg^{-1} based on 4e/FeS_2 (assuming complete reaction with four Li^+ to form the product Li_2S and amorphous Fe), the possibility of overcharge protection and cooling of the battery in larger EV type batteries at high discharge rate, although it has been commercialized as a high-capacity electrode material in lithium ion primary batteries and investigated as a promising secondary battery cathode in Li-Al/FeS_2 batteries with good reversibility at 400℃ as well. [17,18] Nevertheless, these appealing attributes of pyrite as cathode material for LIBs stimulate the resurgent research interest to address energy storage challenges today and for the future due to the continuously surging demand for environmental issues as well as for emerging large-scale energy applications such as low-emission electric vehicles (EV), hybrid electric vehicles (HEVs), renewable power plants and electric grids.

Unfortunately, the lithiation/delithiation of pyrite cathode to form Fe and Li_2S has thoroughly been characterized with limited reversibility at ambient temperature[19], which severely handicap the capacity retention of pyrite electrode. Also, it brings about the drastic volume variation due to the large density difference between FeS_2 (d = 5.0 g cm^{-3}) and Li_2S (d = 1.67 g cm^{-3}), resulting in the fast capacity fading upon electrochemical cycling, which is similar to Li/S battery. In addition, the sluggish kinetics for charge transfer and ionic diffusion, as well as high intrinsic resistance also induces additional performance degradation of pyrite-based electrodes, especially at high current densities.[19] Therefore, the fabrication of truly durable pyrite electrode with satisfactory high-rate capability and high specific capacity is still a great challenge.

So far, many efforts have been made to circumvent the above issues to improve the capacity and rate capability of pyrite electrode. Nanostructuring has been shown as an effective approach to obtain the high initial capacity for pyrite electrode by reducing inner resistance and Ohmic loss, increasing electrode/electrolyte contact area and shortening the path lengths for transport of electrons. [5,20–23] However, poor reversibility was observed due to less intercalation stress[24,25], compared to microsized pyrite electrode[23,26–29], resulting in quick capacity fading. Furthermore, the hollow pyrite electrode exhibited

significantly improved electrochemical performance by enhancing surface-to-volume ratio and reducing transport lengths for both mass and charge transport, making an ideal host for reversible Li^+ intercalation with a high stability.[28,30–33] Meanwhile, hollow structure also could accommodate the large volumetric expansion of FeS_2 during lithiation, thus preserving the structural integrity, as applied to the confinement of intermediate polysulfides in Li/S batteries.[34] Keeping all these in mind, herein, we reported a novel hierarchical nanostructured pyrite hollow microsphere in which nanoflakes were self-assembled hierarchically based on Ostawald ripening[35]. In theory, such a unique hierarchical nanostructured hollow microsphere is expected to manifest greatly improved electrochemical performance of pyrite cathode for LIBs because of the integration of several advantageous structural features, which would be impetus to develop the pyrite-based electrode with high capacity and rate capability. Benefited from the enhanced structural stability and kinetics for lithium storage, the as-obtained pyrite electrode in this work exhibited an exceptionally stable capacity retention of ~ 400 mAh g^{-1} at 1 C.

Experimental

Preparation and characterization of hierarchical nanostructured pyrite hollow microspheres

The preparation of the hierarchical nanostructured pyrite hollow microsphere was carried out via one-pot solvothermal process. In a typical synthesis, 4 mmol of sulfur powder was dissolved in 10 mL of triethanolamine and 2 mmol of $FeSO_4 \cdot 7H_2O$ was dissolved in 20 mL of deionized water. Then the above solutions were mixed well under eletromagnetic stirring. Subsequently, the mixed solution was transferred into a 50 mL sealed Teflon-lined stainless steel autoclave and maintained at 180 ° C for 12 h. After reaction, the autoclave was cooled to room temperature naturally. The resulting precipitates were collected by centrifugation and then washed with deionized water and absolute ethanol several times, respectively. Finally, the black pyrite precipitated was dried in the oven at 80° C for 10 h, and the hierarchical nanostructured pyrite hollow microspheres were obtained. Other comparative experiments by changing the sulfur powder dosage and reaction time were the same procedure as the above otherwise specified.

X-ray diffraction (XRD) patterns were recorded on a Shimadzu XRD-6000 diffractometer operating with Cu Kα radiation (λ= 1.5418 Å) at a scanning step of 2º per minute. Field emission scanning electron microscopy (FESEM) images were taken by a Hitachi SEM. The samples were prepared by sonicating the products in absolute ethanol and evaporating one drop of suspension on conductive adhesive. The transmission electron microscopy (TEM) images and high-resolution transmission electron microscopy (HRTEM) images were acquired using a JEOL JEM-2010 HRTEM operating with an acceleration voltage of 200 kV. The samples were prepared by dipping an amorphous carbon-copper grid in a dilute solution of samples dispersed in absolute ethanol. Energy-dispersive spectrum (EDS) was taken on Hitachi field emission scanning electron microscopy.

Electrochemical measurement

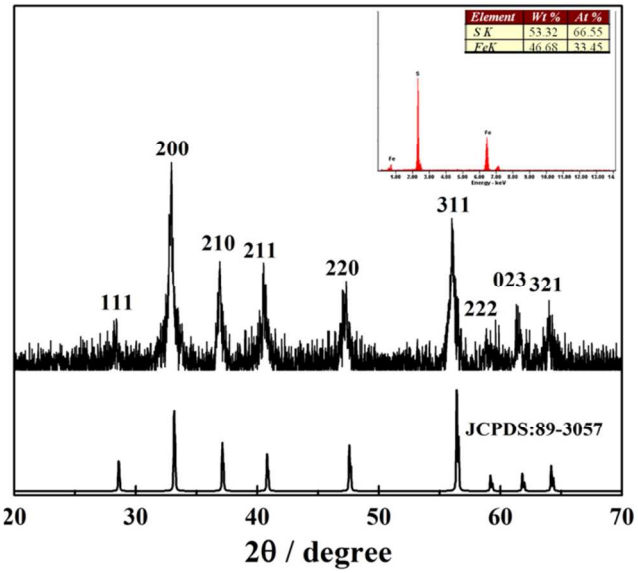

Fig. 1 XRD pattern of the as-obtained pyrite in comparison with reference diffractogram of cubic pyrite. Inset: EDS pattern of pyrite.

The hierarchical nanostructured pyrite hollow microsphere powder was mixed with acetylene black and polyvinylidene diuoride (PVDF) in a weight ratio of 70:20:10, with N-methyl pyrrolidone (NMP) as a dispersant. Then, the slurry was pasted on aluminium foil strip of 1 cm^2 in apparent area and approximately 2.5 mg in weight. The strips were dried at 80℃ for 24 h before use. 2016 coin-type cells were assembled in a glove box filled with high pure Ar using lithium metal as the counter electrode, and microporous polypropylene (Celgard®2325) as the separator and 1M $LiPF_6$ in a mixed solvent of ethylene carbonate (EC) and diethyl carbonate (DEC) (1:1, v/v) as electrolyte. The measurements of electrochemical performance were carried out on a program-controlled Battery Test System (Land®, Wuhan, China) at room temperature. The cyclic voltammetry (CV) was conducted in a three-electrode cell with lithium foil as counter and reference electrodes by using a CHI660B Electrochemical Work-station (Chenghua, Shanghai, China) at room temperature. The electrochemical property of the hierarchical nanostructured pyrite hollow microspheres was measured by a program-controlled Battery Test System (Land®, Wuhan, China).

Results and discussion

Following the typical reaction conditions, trienthanolamine was used to dissolve sulfur powder and $FeSO_4 \cdot 7H_2O$ was dissolved in deionized water. The phase and purity of the as-obtained pyrite was determined using powder XRD analysis, see Fig. 1. All the diffraction peaks observed in this pattern can be indexed as the pure cubic phase of pyrite with a lattice constant of a= 5.417 Å, which is in good agreement with the value given in the standard card (JSPDS card No. 89-3057). No other iron-sulfur related phases, such as marcasite (FeS_2), pyrrhotite ($Fe_{1-x}S$), troilite (FeS), or greigite (Fe_3S_4), are observed, which indicates that the sample is pure. The strong and sharp diffraction peaks illuminate the high crystallization nature of the sample. Moreover, EDS was performed to further determine the chemical composition. The results inserted in Fig. 1 reveal that no other element is observed except Fe and S. Furthermore, the quantification of the peaks

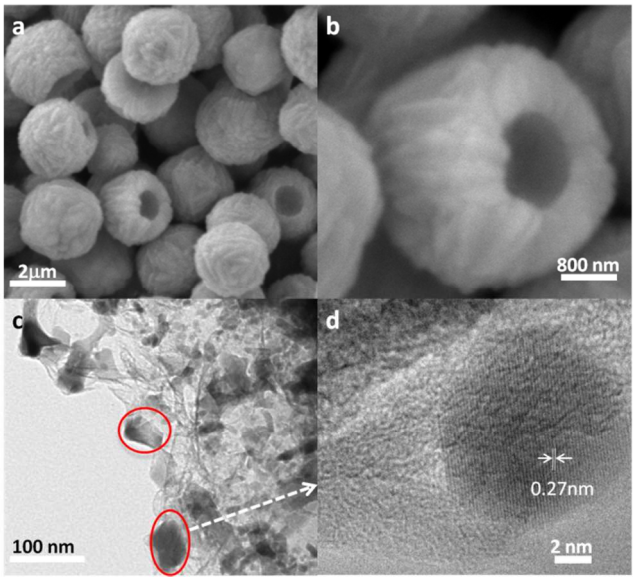

Fig. 2 FESEM and HRTEM images of the as-obtained pyrite; (a) lower magnification, and (b) higher magnification, (c) HRTEM image and (d) lattice –resolved HRTEM image.

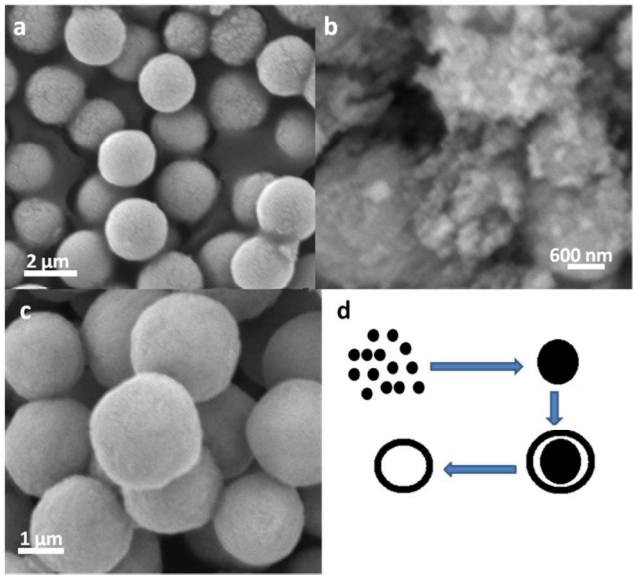

Fig. 3 SEM images of the pyrite prepared at 180℃ for (a) 8 mmol sulfur powder and 12 h, (b) 4 mmol sulfur powder and 1 h, (c) 4 mmol sulfur powder and 6 h, and (d) schematic illustration of the formation of the hierarchical nanostructured pyrite hollow microspheres.

shows that the molar ratio of S and Fe is 1.99, which is quite close to the refinement results and stoichiometric FeS_2. In addition, based on the Debye–Scherrer equation, the crystallite sizes could be calculated approximately at the highest peak (2 0 0) to be ca.26.0 nm from XRD pattern, which is the basic particle unit to form hollow microsphere. SEM image shown in Figure 2a illustrates that the sample prepared at 180℃ for 12 h is composed of uniform hollow microsphere structures. From the typical magnified SEM image (Fig.2b), it is observed that the as-prepared pyrite hollow microspheres are about 2 μm in diameter and the shells are about 500 nm in thickness. Furthermore, it could also be seen clearly that the shell is comprised of nanoflakes with the diameter of about 20 nm, which is revealed further by the magnified TEM images from the edge of a microsphere (Fig. 2c). The HRTEM image of nanoflake pyrite particle exhibits clear regular lattice fringes with a spacing of 0.27 nm, which corresponds to the (200) plane of pyrite (Fig. 2d).

To shed an insight on the formation mechanism of hierarchical nanostructured pyrite hollow microsphere, several typical experiments were carried out by changing the S dosage and reaction time under conditions otherwise the same. The solvent trienthanolamine employed in our synthesis is thought to serve as reducing agent for the reduction of sulfur powder to S^{2-}, which is similar to those reported that ethanol, EG and DMF might act as reducing agents at high temperature.[36,37] It is generally believed that S as sulfur source could steadily supply S^{2-} in a controllable way in the whole process to favour the formation of regular particles[38,25]. Moreover, the dosage of S is also important in tuning the morphologies. When twice as much as S dosage for the synthesis of hierarchical nanostructured pyrite microsphere was used, the solid pyrite microsphere was produced (Fig. 3a), which implies that excess S is unfavorable for the formation of pyrite hollow structure in that there may be no time enough for the solid core to evacuate to form hollow microsphere due to quick reaction. As shown in Fig. 3b and c, at the reaction time of 1 h, the microsphere composed of nanoparticles with the diameter of about 20 nm packed loosely. When the reaction was prolonged to 6 h, the solid microsphere was formed due to the aggregation of the primary nanoparticles. With the reaction evolved further, the core-shell structures (not shown here) and hollow structures were produced finally owing to the evacuation of the solid core and the generation interior space. The evolution of hierarchical nanostructured pyrite hollow microsphere is almost consistent with Ostwald ripening formation mechanism for the hollow microspheres[39–41], as shown in Fig.3d for the schematic illustration of the formation of the hierarchical nanostructured pyrite hollow microspheres.

The electrochemical performance of the as-obtained pyrite as cathode material for lithium ion battery was evaluated in coin test cells using lithium as the counter and reference electrode between 1.0 and 2.5 V (*vs.* Li^+/Li) at ambient temperature. As shown in Fig. 4a for the typical charge-discharge curves in the first three cycles at 0.1 C (1 C = 890 mA g^{-1} for pyrite), the as-obtained pyrite electrode exhibits an initial discharge capacity of 886.3 mAh g^{-1}, which is close to the theoretical capacity (890 mAh g^{-1}) of pyrite, indicating almost 100% utilization of the active specie. This may be attributed to hierarchical nanostructure of pyrite which affords a shorter Li^+ and electron transport pathway, improved conversion reaction kinetics, and better utilization of the active species upon discharge and charge. Meanwhile, the initial discharge curve of pyrite electrode present one plateau at 1.5 V followed by a sharp voltage drop due to the ohmic potential drop with lithium insertion and a rise of the Fermi level with respect to the conduction band of pyrite, while the second discharge curve onwards shows an another plateau at approximately 2.0 V, indicating a change in the mechanism of pyrite reduction. According to previous work[42], the lithiation of pyrite involves two reactions, which can occur at one or two voltage depending on the kinetics of the system.

$$FeS_2 + 2Li^+ + 2e \rightarrow Li_2FeS_2 \quad (1)$$

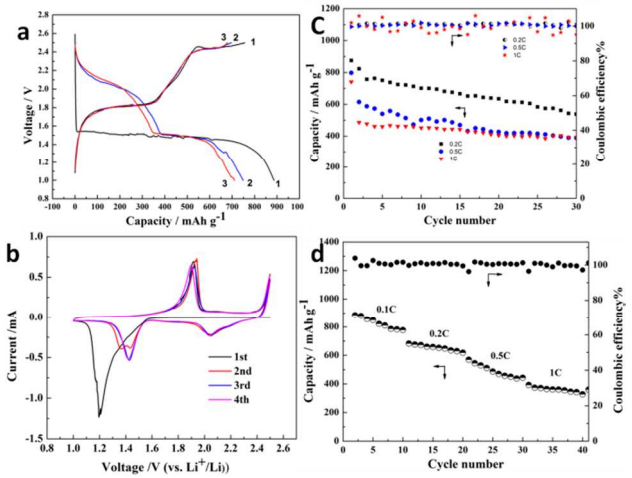

Fig. 4 Electrochemical performances of the as-obtained pyrite electrodes: (a) charge-discharge profiles at 0.1 C rate for the first three cycles; (b) cyclic voltammograms for the as-obtained pyrite with scan rate of 0.2 mV s^{-1} between 1 and 4.5 V for the first three cycles; (c) cycling stability and Coulombic efficiency up to 30 cycles at different rates and (d) consecutive cycling behaviour and their Coulombic efficiency at different rates.

$$Li_2FeS_2 + 2Li^+ + 2e \rightarrow Fe + 2Li_2S \quad (2)$$

Thus, the initial lithiation of pyrite in this work involves one-voltage step reduction of pyrite (direct formation of Li_2S and Fe) due to the slow diffusion of Li^+ into pyrite at ambient temperature and the formation of intermediate phase is suppressed, giving rise to a lithiation peak at 1.2 V in the first scanning cyclic voltammogram (Fig. 4b) of pyrite cathode at a scan rate 0.2 mV s^{-1} between 1 and 2.5 V. In the subsequent cycling, the lithiation involves two-voltage step with the nucleation and growth of intermediate phase in samples, resulting in the two lithiation peaks at 1.2 and 2.0 V in the subsequent scanning cyclic voltammograms (Fig. 4b) of pyrite cathode, which is in agreement with the literature[43–46]. Two charge plateaus at 1.8 and 2.45 V in all the cycles in the charge-discharge curves (Fig. 4a) are indexed to the formation of $Li_{2-x}FeS_2$[42], corresponding to the oxidation peak at ~ 1.9 V in cyclic voltammograms (Fig. 4b) of pyrite cathode. As such, in the first delithiation cycle, only $Li_{2-x}FeS_2$ ($0 < x < 8$) is formed and pyrite is not recovered when recharged to 2.5 V, as the delithiation peak area is clearly smaller than the first lithiation peak area. In subsequent cycles, the cycling appears to be quite reversible, as the lithiation and delithiation peaks were almost the same, i. e.[5,42,47]

$$Li_{2-x}FeS_2 + (2+x)\,Li^+ + (2+x)e^- \rightleftharpoons Fe + 2Li_2S\ (0 < x < 0.8) \quad (3)$$

which rules out other electrochemical processes such as cycling of a pure Li_2S cathode or a sulfur cathode. This is further verified by the discharge-charge cycling tests. As shown in Fig. 4c, pyrite electrode shows an initial discharge capacity of 875.4, 797.7, 741.8 mA h g^{-1} at 0.2, 0.5, 1 C, respectively. After the first cycle, it shows a very good cycling stability and retains a discharge capacity of 537.2, 389.3 and 392.7 mAh g^{-1} at 0.2 C, 0.5 C and 1 C, respectively, after 30 cycles. Furthermore, the cycling performance of the as-obtained pyrite electrode at different charge/discharge rates, measured after 5 cycles at each rate from 0.1 to 1 C in an ascending order, was carried out, as shown in Fig. 4d. The pyrite electrode presents excellent cycling stability at each rate, and reversible capacities were measured to be around 800, 660, 480 and 370 mAh g^{-1} at the rate of 0.1, 0.2, 0.5, and 1 C, respectively. Meanwhile, high average Coulombic efficiency is exhibited (100%, Fig. 4c and d). To the best of our knowledge, such good cycling stability and performance of Li/pyrite cell using liquid electrolyte at ambient temperature has not been reported before except for the FeS_2-Li_2S cell[48]. This might be due to the unique pyrite structure with hierarchical hollow microsphere composed of nanoflakes. As demonstrated by many researchers[5,26–28], microsized pyrite is more favorable to the cycling performance of pyrite electrode compared to the nanosized one. On the other hand, the hierarchical hollow structure of pyrite might prevent diffusion and agglomeration of the product Fe nanoparticle at ambient temperature, as using a variety of polymer[49,50] or solid electrolyte[47] to circumvent this issue. Also, as used in Li/S battery[34,51] to address the sulfur swelling upon discharge and Li_2S irreversibility using liquid electrolyte, the hollow structure is beneficial to avoiding swelling upon discharge due to the small density of Li_2S and to Li_2S irreversibility. As such, this hierarchical hollow structure of pyrite could make Eq.(3) better reversible after the first cycle.

Conclusions

On account of the discharge-charge mechanism of Li/pyrite battery documented well in the literature, a strategy to solve the reversibility of Li/pyrite battery at ambient temperature was proposed in which the hierarchical nanostructured pyrite hollow microsphere was designed in this work. Based on Ostwald ripening, using sulfur powder as sulfur source and triethanolamine as both solvent and reducing agent, the hierarchical pyrite hollow microsphere with the diameter of 2 μm and the shell thickness of 500 nm, which was composed of nanoflakes, was fabricated successfully. The as-obtained pyrite electrode using liquid electrolyte at ambient temperature delivered an initial discharge capacity of 886.3 mAh g^{-1}, suggesting almost 100% utilization of the active specie via one-voltage step reduction of pyrite in the initial lithiation of pyrite, which is one of the highest values in the reported results[52]. This may mainly be attributed to the nanoflake unit of pyrite. After the first cycle, pyrite electrode exhibited a good reversibility due to the reaction of $Li_{2-x}FeS_2$ and Li^+ to yield Fe and Li_2S, which is different mechanism from the first cycle, resulting good cycling stability and performance of pyrite electrode in subsequent cycles. After 30 cycles, the discharge capacity still retained to be 392.7 mAh g^{-1} at 1C rate, which is much higher than that of the current $LiCoO_2$ intercalation cathode material (140 mAh g^{-1}), enabling the nano-pyrite cathode to have comparable discharge energy density to the theoretical energy density of $LiCoO_2$ cathode. All these could be dissected by the unique structure with the hierarchical nanostructured hollow microsphere. We hope that this work can serve as an impetus for further research efforts aiming to utilize earth-abundant pyrite cathode material to increase the energy storage of Li-ion batteries.

Acknowledgements

This work is supported by Education Science Foundation of

Hubei Province (No. Q20091806), Project of Chinese Ministry of Education (No. 208088).

Notes and References

Innovation Center for Nanomaterials in Energy and Medicine (ICNEM), School of Chemical and Environmental Engineering, Wuhan Polytechnic University, Hubei 430023, P. R. China.Fax: +86-27-83943956; Tel: +86-27-83943956; E-mail; icnem@hotmail.com.

1. A. Ennaoui, S. Fiechter, C. Pettenkofer, N. Alonso-Vante, K. Büker, M. Bronold, C. Höpfner, and H. Tributsch, *Sol. Energy Mater. Sol. Cells*, 1993, **29**, 289–370.
2. H. A. Macpherson and C. R. Stoldt, *ACS Nano*, 2012, **6**, 8940–8949.
3. C. Wadia, Y. Wu, S. Gul, S. K. Volkman, J. Guo, and A. P. Alivisatos, *Chem. Mater.*, 2009, **21**, 2568–2570.
4. P. P. Altermatt, T. Kiesewetter, K. Ellmer, and H. Tributsch, *Sol. Energy Mater. Sol. Cells*, 2002, **71**, 181–195.
5. J.-W. Choi, G. Cheruvally, H.-J. Ahn, K.-W. Kim, and J.-H. Ahn, *J. Power Sources*, 2006, **163**, 158–165.
6. E. Peled, D. Golodnitsky, G. Ardel, J. Lang, and Y. Lavi, *J. Power Sources*, 1995, **54**, 496–500.
7. D. Zhang, X. L. Wang, Y. J. Mai, X. H. Xia, C. D. Gu, and J. P. Tu, *J. Appl. Electrochem.*, 2012, **42**, 263–269.
8. A. Ennaoui and H. Tributsch, *Sol. Cells*, 1984, **13**, 197–200.
9. X. Chen, Z. Wang, X. Wang, J. Wan, J. Liu, and Y. Qian, *Inorg. Chem.*, 2005, **44**, 951–954.
10. Q.-H. Huang, T. Ling, S.-Z. Qiao, and X.-W. Du, *J. Mater. Chem. A*, 2013, **1**, 11828.
11. M. Cabán-Acevedo, D. Liang, K. S. Chew, J. P. DeGrave, N. S. Kaiser, and S. Jin, *ACS Nano*, 2013, **7**, 1731–1739.
12. Y. Hu, Z. Zheng, H. Jia, Y. Tang, and L. Zhang, *J. Phys. Chem. C*, 2008, **112**, 13037–13042.
13. Y. Bai, J. Yeom, M. Yang, S.-H. Cha, K. Sun, and N. A. Kotov, *J. Phys. Chem. C*, 2013, **117**, 2567–2573.
14. M. Cabán-Acevedo, M. S. Faber, Y. Tan, R. J. Hamers, and S. Jin, *Nano Lett.*, 2012, **12**, 1977–1982.
15. M. Nath, A. Choudhury, A. Kundu, and C. N. R. Rao, *Adv. Mater.*, 2003, **15**, 2098–2101.
16. P. Gao, Y. Xie, L. Ye, Y. Chen, and Q. Guo, *Cryst. Growth Des.*, 2006, **6**, 583–587.
17. Z. Tomczuk, B. Tani, N. C. Otto, M. F. Roche, and D. R. Vissers, *J. Electrochem. Soc.*, 1982, **129**, 925–931.
18. S. K. Preto, Z. Tomczuk, S. von Winbush, and M. F. Roche, *J. Electrochem. Soc.*, 1983, **130**, 264–273.
19. J. Cabana, L. Monconduit, D. Larcher, and M. R. Palacín, *Adv. Mater.*, 2010, **22**, E170–E192.
20. Y. Shao-Horn and Q. C. Horn, *Electrochimica Acta*, 2001, **46**, 2613–2621.
21. X. Feng, X. He, W. Pu, C. Jiang, and C. Wan, *Ionics*, 2007, **13**, 375–377.
22. I.-S. Ahn, D. W. Kim, D. K. Kang, and D.-K. Park, *Met. Mater. Int.*, 2008, **14**, 65–70.
23. D. Zhang, J. P. Tu, J. Y. Xiang, Y. Q. Qiao, X. H. Xia, X. L. Wang, and C. D. Gu, *Electrochimica Acta*, 2011, **56**, 9980–9985.
24. X. Zhang, W. Shyy, and A. Marie Sastry, *J. Electrochem. Soc.*, 2007, **154**, A910.
25. D. Wang, Q. Wang, and T. Wang, *CrystEngComm*, 2010, **12**, 3797.
26. L. Montoro, *Solid State Ion.*, 2003, **159**, 233–240.
27. S. Grugeon, S. Laruelle, R. Herrera-Urbina, L. Dupont, P. Poizot, and J.-M. Tarascon, *J. Electrochem. Soc.*, 2001, **148**, A285–A292.
28. K. M. Shaju, F. Jiao, A. D?bart, and P. G. Bruce, *Phys. Chem. Chem. Phys.*, 2007, **9**, 1837.
29. Y. J. Choi, N. W. Kim, K. W. Kim, K. K. Cho, G. B. Cho, H. J. Ahn, J. H. Ahn, K. S. Ryu, and H. B. Gu, *J. Alloys Compd.*, 2009, **485**, 462–466.
30. X. Lai, J. E. Halpert, and D. Wang, *Energy Environ. Sci.*, 2012, **5**, 5604.
31. I. Moriguchi, R. Hidaka, H. Yamada, T. Kudo, H. Murakami, and N. Nakashima, *Adv. Mater.*, 2006, **18**, 69–73.
32. Q. Wang, L. Jiao, Y. Han, H. Du, W. Peng, Q. Huan, D. Song, Y. Si, Y. Wang, and H. Yuan, *J. Phys. Chem. C*, 2011, **115**, 8300–8304.
33. D. Zhang, J. Xiang, Y. Zhu, G. Li, J. Jin, G. Wu, J. Weng, X. Mao, Z. Liu, and X. Hu, *J. Nanosci. Nanotechnol.*, 2014, **14**, 6095–6102.
34. X. Ji and L. F. Nazar, *J. Mater. Chem.*, 2010, **20**, 9821.
35. M. Kahlweit, *Adv. Colloid Interface Sci.*, 1975, **5**, 1–35.
36. Y. Xiong, J. M. McLellan, J. Chen, Y. Yin, Z.-Y. Li, and Y. Xia, *J. Am. Chem. Soc.*, 2005, **127**, 17118–17127.
37. F. Bonet, V. Delmas, S. Grugeon, R. Herrera Urbina, P.-Y. Silvert, and K. Tekaia-Elhsissen, *Nanostructured Mater.*, 1999, **11**, 1277–1284.
38. D.-W. Wang, Q.-H. Wang, and T.-M. Wang, *CrystEngComm*, 2010, **12**, 755–761.
39. B. Liu and H. C. Zeng, *Small*, 2005, **1**, 566–571.
40. J. Li and H. C. Zeng, *J. Am. Chem. Soc.*, 2007, **129**, 15839–15847.
41. Y. Zhao and L. Jiang, *Adv. Mater.*, 2009, **21**, 3621–3638.
42. R. Fong, J. R. Dahn, and C. H. W. Jones, *J. Electrochem. Soc.*, 1989, **136**, 3206–3210.
43. C. H. W. Jones, P. E. Kovacs, R. D. Sharma, and R. S. McMillan, *J. Phys. Chem.*, 1991, **95**, 774–779.
44. Y. Yamaguchi, T. Takeuchi, H. Sakaebe, H. Kageyama, H. Senoh, T. Sakai, and K. Tatsumi, *J. Electrochem. Soc.*, 2010, **157**, A630–A635.
45. D. A. Totir, I. T. Bae, Y. Hu, M. R. Antonio, M. A. Stan, and D. A. Scherson, *J. Phys. Chem. B*, 1997, **101**, 9751–9756.
46. C. H. W. Jones, P. E. Kovacs, R. D. Sharma, and R. S. McMillan, *J. Phys. Chem.*, 1990, **94**, 832–836.
47. T. A. Yersak, H. A. Macpherson, S. C. Kim, V.-D. Le, C. S. Kang, S.-B. Son, Y.-H. Kim, J. E. Trevey, K. H. Oh, C. Stoldt, and S.-H. Lee, *Adv. Energy Mater.*, 2013, **3**, 120–127.
48. T. Takeuchi, H. Kageyama, K. Nakanishi, Y. Inada, M. Katayama, T. Ohta, H. Senoh, H. Sakaebe, T. Sakai, K. Tatsumi, and others undefined, *J. Electrochem. Soc.*, 2011, **159**, A75–A84.
49. D. Golodnitsky and E. Peled, *Electrochimica Acta*, 1999, **45**, 335–350.
50. E. Strauss, D. Golodnitsky, K. Freedman, A. Milner, and E. Peled, *J. Power Sources*, 2003, **115**, 323–331.
51. V. S. Kolosnitsyn and E. V. Karaseva, *Russ. J. Electrochem.*, 2008, **44**, 506–509.
52. L. Li, M. Cabán-Acevedo, S. N. Girard, and S. Jin, *Nanoscale*, 2014, **6**, 2112.